Journal of Physics and Chemistry of Solids 179 (2023) 111429

Contents lists available at ScienceDirect

Journal of Physics and Chemistry of Solids

journal homepage: www.elsevier.com/locate/jpcs

The pressure response of SnS_xSe_{2-x} tin dichalcogenide alloys studied by Raman spectroscopy

N. Sorogas [a], M. Menelaou [b], A.N. Anagnostopoulos [a], K. Papagelis [a], D. Christofilos [c], J. Arvanitidis [a,*]

[a] Physics Department, Aristotle University of Thessaloniki, 54124, Thessaloniki, Greece
[b] Department of Chemical Engineering, Cyprus University of Technology, 3036, Limassol, Cyprus
[c] School of Chemical Engineering & Laboratory of Physics, Faculty of Engineering, Aristotle University of Thessaloniki, 54124, Thessaloniki, Greece

ARTICLE INFO

Keywords:
Tin dichalcogenide alloys
2D materials
Raman spectroscopy
High pressure

ABSTRACT

High-pressure Raman spectroscopic experiments were conducted in a diamond anvil cell to investigate the pressure response of the phonon modes of SnS_xSe_{2-x} ($x = 0.6, 0.8, 1$) tin dichalcogenide alloys up to 8 GPa. Owing to the two-mode behavior of the E_g and A_{1g} modes in these ternary alloys, up to four Raman bands are observed at ambient conditions and the frequency evolution of three of them {E_g($SnSe_2$-like), A_{1g}($SnSe_2$-like) and A_{1g}(SnS_2-like)} is followed with pressure. With increasing pressure, all the Raman bands shift quasi-linearly and reversibly to higher frequencies, reflecting the bond stiffening due to the volume reduction and the absence of any phase transition. Despite the stronger intralayer covalent bonding compared to the much weaker interlayer van der Waals interactions along the *c*-axis, the in-plane E_g($SnSe_2$-like) mode has larger pressure coefficient than those of the two stronger in intensity A_{1g} modes along the *c*-axis. The pressure coefficient of the A_{1g}(SnS_2-like) mode gradually increases from 3.60 to 3.93 $cm^{-1}GPa^{-1}$ with increasing sulfur content (x). On the other hand, the pressure coefficient of the A_{1g}($SnSe_2$-like) mode decreases from 3.08 to 2.72 $cm^{-1}GPa^{-1}$ with increasing x. The extracted Grüneisen parameters of all the A_{1g} Raman peaks indicate the stronger Sn–S interaction along the *c*-axis compared to that of Sn–Se.

1. Introduction

Tin-selenides (Sn_xSe_y) and tin-sulfides (Sn_xS_y) have attracted great attention in recent years due to their important physicochemical, optical, and thermal properties, emerging as potential candidates for a plethora of practical and novel applications [1–3]. These compounds are a combination of a post-transition metal (Sn) and a chalcogen (S/Se) atom and, taking into account the natural abundance of the constituent elements, they are most importantly low-cost, non-toxic and eco-friendly materials. Varying compositions of tin-based chalcogenides are promising for the future of intelligent nanoelectronics, offering adaptable chemical behavior for the fabrication of alloys, heterostructures, composites and hybrids [4]. Other commercial applications include solar cells, photodetectors, field effect transistors (FETs), flexible sensors, and even antimicrobial nanostructures, owing much to their strong anisotropic properties and thickness-dependent responsivity [5–9].

Widely studied compounds belonging to the tin chalcogenide family are the SnS_2 and $SnSe_2$ dichalcogenides, being analogous to the transition metal dichalcogenides (TMDs) [10,11]. These compounds are layered semiconductors, where in each layer, the Sn atoms are octahedrally coordinated to the chalcogen atoms, with comparable lattice constants [12–14]. At ambient conditions, they commonly crystallize in the $P\bar{3}m1$ (D^3_{3d}) space group with a hexagonal close-packed CdI_2-type structure. They also present different polytypes, depending on the preparation and growth methods, according to the stacking order of the layers [15–20]. In this system, strong covalent intralayer bonds are formed within X-Sn-X (X = S, Se) layers that are stacked through weak interlayer van der Waals interactions [10]. Therefore, the individual tin dichalcogenide layers can be quite easily isolated by mechanical exfoliation and thus, can serve as two dimensional (2D) building blocks for the construction of novel versatile nanostructures [21]. Both $SnSe_2$ and SnS_2 possess indirect energy bandgaps of ~1.3 and ~2.2 eV, respectively, while, being isostructural compounds, the formation of tin dichalcogenide alloys with compositions SnS_xSe_{2-x} ($0 < x < 2$) and

* Corresponding author.
E-mail address: jarvan@physics.auth.gr (J. Arvanitidis).

https://doi.org/10.1016/j.jpcs.2023.111429
Received 29 November 2022; Received in revised form 11 April 2023; Accepted 7 May 2023
Available online 8 May 2023

tunable bandgap is feasible [22]. Such alloys are suitable for applications where high, application-specific optical transmittance or absorbance is required, while they also display adequate piezoelectric properties and catalytic activities that are necessary for the design of functional optoelectronic devices [23–27]. For example, it has been recently reported that SnS_xSe_{2-x} phototransistors exhibit high photoresponsivity with ultra-high photogain, fast response time and specific detectivity [27]. Moreover, an optical modulator based on tin dichalcogenide alloy nanosheets was successfully incorporated as a saturable absorber into a stable passively Q-switched fiber laser, taking advantage of the optical nonlinearity of SnS_xSe_{2-x} and revealing the potential of this system in ultrafast photonics [28].

Tin-based chalcogenides undergo significant changes in their structural and electronic properties upon pressure application and/or as a function of temperature, hosting new superconducting, charge density wave (CDW) or topologically non-trivial phases [29–32]. However, although the binary SnS_2 and $SnSe_2$ tin dichalcogenides have been extensively investigated so far, their structural stability and optical properties under high pressure remain still quite unclear. More specifically, early experimental and theoretical studies of the optical properties and the band structure of 2H–SnS_2 and 4H–SnS_2 polytypes at 77 K and 273 K and as a function of hydrostatic pressure were reported by M. J. Powell et al., demonstrating their anisotropic nature and the closing of their bandgaps with pressure that strongly depends on the polytype structure and temperature [33,34]. M. Filsø et al. investigated the effect of high pressure on the structural and electronic properties of 2H SnS_2 single crystals ($P\bar{3}m1$ space group) up to 20 GPa by joint high-pressure single-crystal X-ray diffraction (XRD) and Density-functional theory (DFT) studies. They reported that the layered structure of the material compresses anisotropically over the whole pressure range, where the compression in the *c*-direction stems solely from the decrease in the interlayer distances, with no structural or semiconductor to semimetal transition up to 20 GPa, despite the continuous reduction of the bandgap, suggesting its complete closure at 33 GPa [35]. Z.V. Borges et al. investigated the structural properties of nanostructured $SnSe_2$ for pressures up to 25.8 GPa and they reported an irreversible phase emerging between 7 and 9 GPa, which is compatible with the orthorhombic TiS_2 cotunnite-type structure [36]. On the other hand, S.V. Bhatt et al. studied the Raman spectrum of SnS_2 and $SnSe_2$ single crystals at high pressures up to 20 GPa and low temperatures down to 80 K and no phase transition was observed [37]. However, A.N. Utyuzh et al. found, also by means of high-pressure Raman spectroscopy, a structural phase transition of 2H–SnS_2 at 3 GPa [38]. G.P. Kafle et al. theoretically predicted a pressure-induced semiconductor-to-metal transition at 6 GPa and 20 GPa for $SnSe_2$ and SnS_2, respectively [29]. Furthermore, K. Nguyen-Cong et al. predicted that $P\bar{3}m1$ $SnSe_2$ is structurally stable up to 18 GPa, becoming metallic at 8 GPa. Above 18 GPa, it becomes thermodynamically metastable and eventually dynamically unstable, decomposing to Sn_3Se_4 and Se [39]. In addition, J. Ying et al. indicated a pressure induced periodic lattice distortion (PLD) for $SnSe_2$ and the formation of a (1/3,1/3,0)-type superlattice above 17 GPa due to the combined effect of strong Fermi surface nesting and electron-phonon coupling [32]. Towards this direction, X. Zhang et al. have shown a pressure-induced coupled structural-electronic transition for the sister compound SnS_2 at 30.2 GPa under non-hydrostatic conditions; the phase transition is delayed by 3 GPa under hydrostatic conditions [40]. Nevertheless, Y. Shi et al. reported the structural stability of 4H–SnS_2 up to 56 GPa [41].

Contrary to the plethora of existing literature reports for the binary SnS_2 and $SnSe_2$ compounds exemplified above, the high-pressure response of ternary tin dichalcogenide alloys remains rather unexplored and most of the studies focus on their composition-dependent structural, thermal, vibrational, and optical properties at atmospheric pressure [42–46]. In this work, the structural stability and the pressure response of the phonon modes of ternary SnS_xSe_{2-x} (x = 0.6, 0.8, 1) alloys upon hydrostatic pressure application up to 8 GPa are examined by means of Raman spectroscopy.

2. Experimental

The layered SnS_xSe_{2-x} (x = 0–2) crystals were synthesized by the vertical Bridgman technique and crystallize in an almost hexagonal lattice with space group $P\bar{3}m1$ (D^3_{3d}), as detailed elsewhere [47]. Raman spectra of the SnS_xSe_{2-x} crystals were recorded in the backscattering geometry using a microscope-equipped single stage spectrometer (LabRAM HR, HORIBA) with a Peltier-cooled charge-coupled device (CCD) detector. For excitation, the 515 nm line of a diode-pumped solid-state laser (Fandango, COBOLT) was focused on the sample by means of a 50× super long working distance objective, while the laser power was kept below 0.3 mW on the focusing spot of ~2 μm in diameter, in order to eliminate any laser-heating effects. By using the 1800 gr/mm grating and a confocal pinhole of 50 μm, the spectral width of the system was ~1 cm^{-1}, while the Raman frequency was calibrated prior to every spectrum accumulation by means of a Ne lamp. High pressure, up to 8 GPa, was generated by a gas membrane type diamond anvil cell (DAC, Almax-easyLab) and calibrated using the ruby fluorescence method [48]. The 4:1 methanol-ethanol mixture was used as the pressure transmitting medium (PTM), which ensures good hydrostatic behavior in the whole pressure range investigated in the present experiments [49].

3. Results and discussion

The Raman spectra at ambient conditions of the ternary SnS_xSe_{2-x} (x = 0.6, 0.8, 1) alloys, along with those of the binary SnS_2 and $SnSe_2$ tin dichalcogenides are illustrated in Fig. 1. The frequency and the relative intensity of the observed Raman peaks are in good agreement with those observed in the literature [44–46,50]. In the case of the binary tin dichalcogenides in the 2H polytype ($P\bar{3}m1$ space group), the unit cell contains three atoms that lead to nine normal modes of vibration, three doubly degenerate E modes (the atomic motions are parallel to the layer) and three non-degenerate A modes (the atomic motions are perpendicular to the layer). At the center of the Brillouin zone (Γ point) the irreducible representations are: $\Gamma = A_{1g} + E_g + 2A_{2u} + 2E_u$. The acoustic modes are of A_{2u} and E_u symmetry, while from the remaining six optical modes, those of $A_{1g} + E_g$ symmetry are Raman-active and

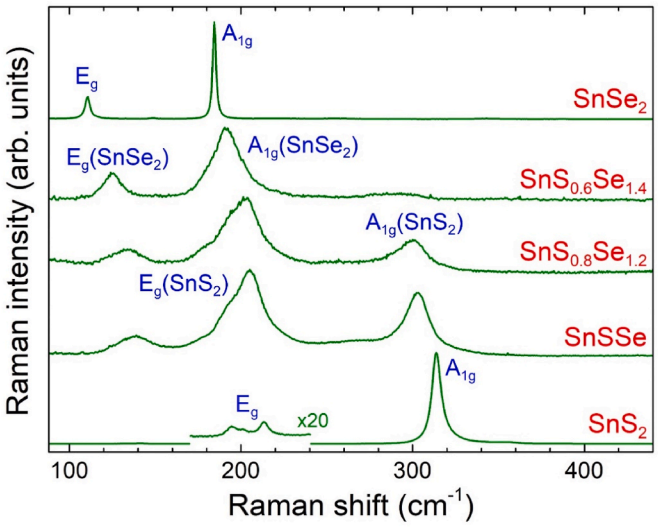

Fig. 1. Raman spectra of the ternary SnS_xSe_{2-x} (x = 0.6, 0.8, 1) alloys at ambient conditions, along with those of the binary SnS_2 and $SnSe_2$. The frequency region around 200 cm^{-1} in the SnS_2 spectrum was multiplied by a factor of 20 for clarity.

those of A_{2u} + E_u are infrared-active [46,50]. In the Raman-active modes, the Sn atom of the intermediate sandwiched sheet out of the three comprising each SnX_2 (X = S, Se) layer of the structure remains stationary because it is located at the center of inversion, while the two chalcogen atoms (S/Se) vibrate anti-phase [37,38,50]. As it can be inferred from Fig. 1, $SnSe_2$ exhibits a strong peak at ~185 cm^{-1}, corresponding to the out-of-plane A_{1g} mode, and a weaker one at ~111 cm^{-1}, attributed to the in-plane E_g mode. In the case of SnS_2, the A_{1g} mode appears at ~314 cm^{-1}, while the Raman peak corresponding to the E_g mode is much weaker. To improve visibility in the corresponding spectrum of Fig. 1, the frequency region around 200 cm^{-1} (where the E_g mode of 2H–SnS_2 is expected) was multiplied by a factor of 20. In accordance with the literature, the weak peak at ~201 cm^{-1} could be assigned to the E_g mode of the 2H polytype [46,50]. However, the presence of the two additional peaks on either side of this peak is a strong indication for the inclusion of other polytypes, like 4H or 18R, in the SnS_2 sample [51,52]. Note that the large separation between the Raman mode frequencies in $SnSe_2$ and SnS_2 comes mostly from the large ratio of the Se and S atomic masses (~2.46) [45].

In the case of the ternary tin dichalcogenide alloys, the broad and asymmetric line shape of the peaks appearing in their Raman spectra (Fig. 1) can be attributed to the random S and Se distribution [22,45,53]. In these dichalcogenide alloys, the E_g and A_{1g} modes exhibit two-mode behavior [44–46], stemming from the clear separation between the corresponding phonon dispersion curves of the binary $SnSe_2$ and SnS_2 compounds [45]. Therefore, up to four bands appear in the Raman spectrum of the studied $SnS_{0.6}Se_{1.4}$, $SnS_{0.8}Se_{1.2}$ and SnSSe alloys, and are attributed, taking into account the existing literature [45,46], to the E_g($SnSe_2$-like), E_g(SnS_2-like, shoulder), A_{1g}($SnSe_2$-like) and A_{1g}(SnS_2-like) modes as shown in Fig. 1. In accordance with this assignment, with increasing S content (x) in the SnS_xSe_{2-x} series, the E_g(SnS_2-like) and the A_{1g}(SnS_2-like) bands gradually gain in intensity at the expense of the E_g($SnSe_2$-like) and the A_{1g}($SnSe_2$-like) Raman bands. At the same time, the frequencies of all the observed Raman bands exhibit moderate blueshifts in going from $SnSe_2$ to SnS_2, as clearly depicted in Fig. 2, where the peak positions of the E_g and A_{1g} modes in the studied SnS_xSe_{2-x} (x = 0–2) dichalcogenides are plotted as a function of x. However, the observed frequency evolution with x cannot be solely explained by the difference in the Se and S atomic masses in the ternary alloys, and the local strain of the trigonal Sn_3Se and Sn_3S pyramids of their crystal structure should be also considered. Namely, the comparison of the SnS_xSe_{2-x} (x = 0–2) lattice constants reported by V.G. Hadjiev et al. [45], gives a gradual decrease of both a and c lattice constants in going from $SnSe_2$ to SnS_2. Thus, in the mixed crystals, the Sn_3Se pyramids experience local compressive strain, while the Sn_3S pyramids are subjected to tensile strain. This difference can partially explain the experimentally observed frequency dependence of the various Raman bands as a function of the S content [45].

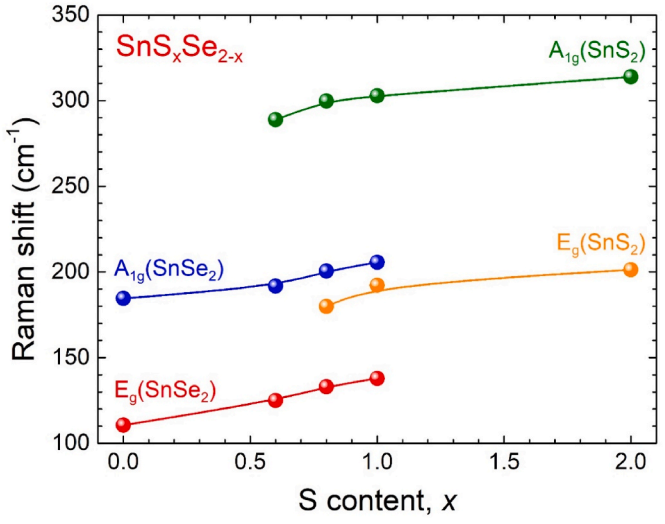

Fig. 2. The frequencies of the E_g and A_{1g} Raman peaks of the SnS_xSe_{2-x} (x = 0–2) dichalcogenides at ambient conditions as a function of the S content, x. Lines through the experimental data are guides to the eye.

Raman spectra of the studied ternary SnS_xSe_{2-x} (x = 0.6, 0.8, 1) alloys at various pressures recorded upon pressure increase are illustrated in Fig. 3. With increasing pressure, all the Raman peaks shift monotonically to higher frequencies, as usually expected due to the volume reduction and the concomitant bond strengthening, without any considerable change in the overall spectrum profile for each alloy up to the highest pressures attained in our experiments (6.3–7.8 GPa). The only exception is the continuous reduction of the relative intensity of the lowest frequency, weak Raman band assigned to the E_g($SnSe_2$-like) mode, compatible with its different symmetry from the other two well-resolved bands attributed to the A_{1g} modes ($SnSe_2$-like and SnS_2-like). For all the studied compounds, these relative intensity changes are reversible upon pressure release and the spectra recorded before and after the corresponding pressure cycle are almost identical.

The frequency evolution of the three well-resolved Raman peaks {E_g($SnSe_2$-like), A_{1g}($SnSe_2$-like) and A_{1g}(SnS_2-like)} with pressure was followed and the corresponding data for $SnS_{0.6}Se_{1.4}$, $SnS_{0.8}Se_{1.2}$ and SnSSe are presented in Fig. 4. The pressure dependence of all frequencies is quasi-linear and fully reversible with decreasing pressure (solid symbols in Fig. 4), excluding the occurrence of any pressure-induced phase transition in the ternary tin dichalcogenide alloys in the pressure range investigated. This is in line with the high pressure Raman studies of the A_{1g} mode frequencies in binary $SnSe_2$ and SnS_2 by S.V. Bhatt et al. [37] and SnS_2 by X. Zhang et al. [40], where there were no alterations in their linear pressure-induced hardening up to 20 GPa or 30 GPa, respectively, and in contrast to the earlier work by A.N. Utyuzh et al. [38], where a reduction of the pressure coefficient of the A_{1g} mode frequency in SnS_2 has been observed for $P > 3$ GPa and attributed to a pressure-induced structural transition.

Linear least-square fits of the frequency *vs* pressure data yield the pressure coefficient values included also in Fig. 4. From these values, it is evident that in all the studied alloys the pressure coefficient of the E_g($SnSe_2$-like) mode frequency is larger than those for the two A_{1g} symmetry modes, ranging from 4.75 to 5.32 $cm^{-1}GPa^{-1}$. This finding is somehow in contrast with the in-plane character of the E_g mode compared to the A_{1g} mode vibration along the c-axis, considering the strong intralayer covalent bonding and the weak van der Waals interactions between the SnX_2 (X = S, Se) layers. However, the results of the present work are in accordance with those of X. Zhang et al. for the binary SnS_2, where the pressure coefficient for the E_g frequency was found to be 5.68 (non-hydrostatic) or 4.90 $cm^{-1}GPa^{-1}$ (hydrostatic conditions), while that of the A_{1g} frequency 3.31 (non-hydrostatic) or 3.25 $cm^{-1}GPa^{-1}$ (hydrostatic conditions) [40]. Moreover, J. Ying et al. reported high pressure Raman data for the E_g and the A_{1g} mode frequency in $SnSe_2$ [32]. Although they do not provide the corresponding pressure coefficient values for a direct comparison, from Fig. 3(b) of their work, illustrating the frequency dependence of the E_g and the A_{1g} modes of $SnSe_2$ as a function of pressure, it is evident that the hardening with increasing pressure of the E_g mode frequency is also faster compared to that of the A_{1g} mode. As for the pressure coefficient of the A_{1g}(SnS_2-like) mode frequency in the studied SnS_xSe_{2-x} alloys, it increases gradually from 3.60 to 3.93 $cm^{-1}GPa^{-1}$ with increasing S content, x. These values lie in the low part of the 3.3–5.2 $cm^{-1}GPa^{-1}$ range reported in the literature for the binary SnS_2 [37,38,40,51]. On the other hand, the pressure coefficient of the A_{1g}($SnSe_2$-like) mode frequency gradually decreases from 3.08 to 2.72 $cm^{-1}GPa^{-1}$ with increasing x, being quite larger than that reported for the binary $SnSe_2$ (1.9 $cm^{-1}GPa^{-1}$) [37], though smaller than those for SnS_2. These findings are compatible with the assignment of the two A_{1g} Raman bands in the ternary alloys.

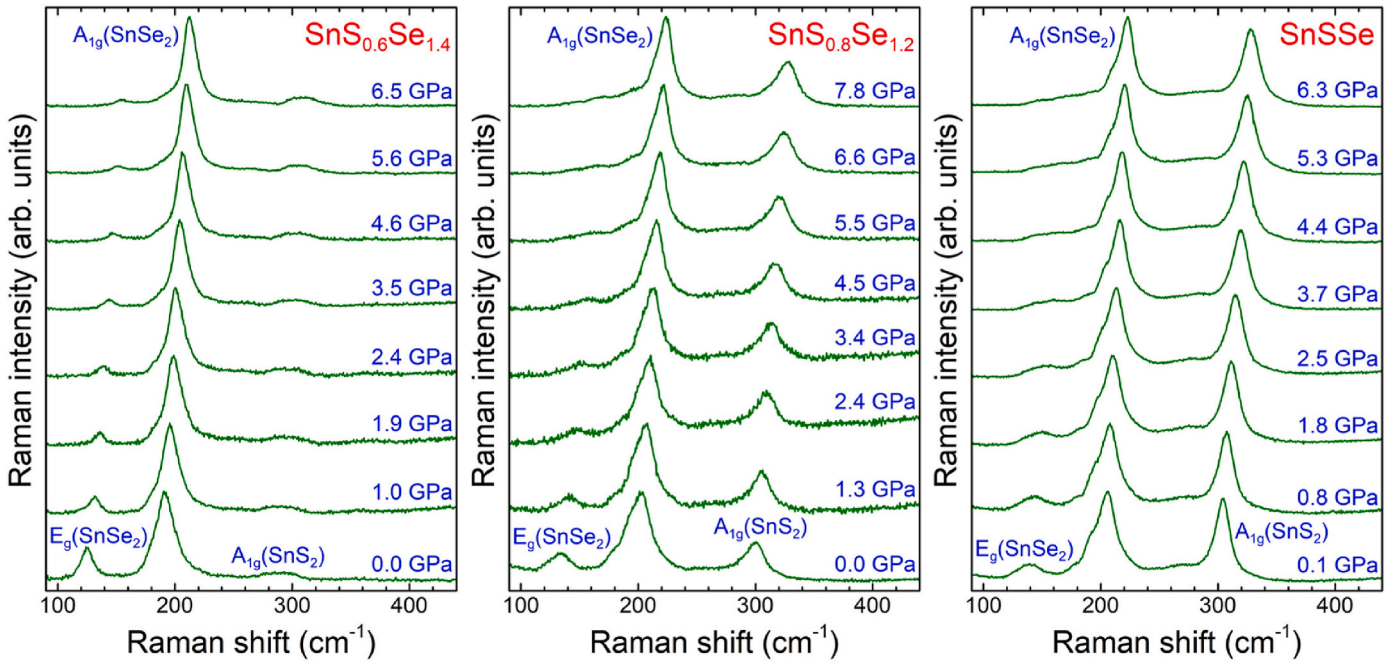

Fig. 3. Representative Raman spectra of the ternary SnS_xSe_{2-x} ($x = 0.6, 0.8, 1$) alloys at various pressures recorded upon pressure increase.

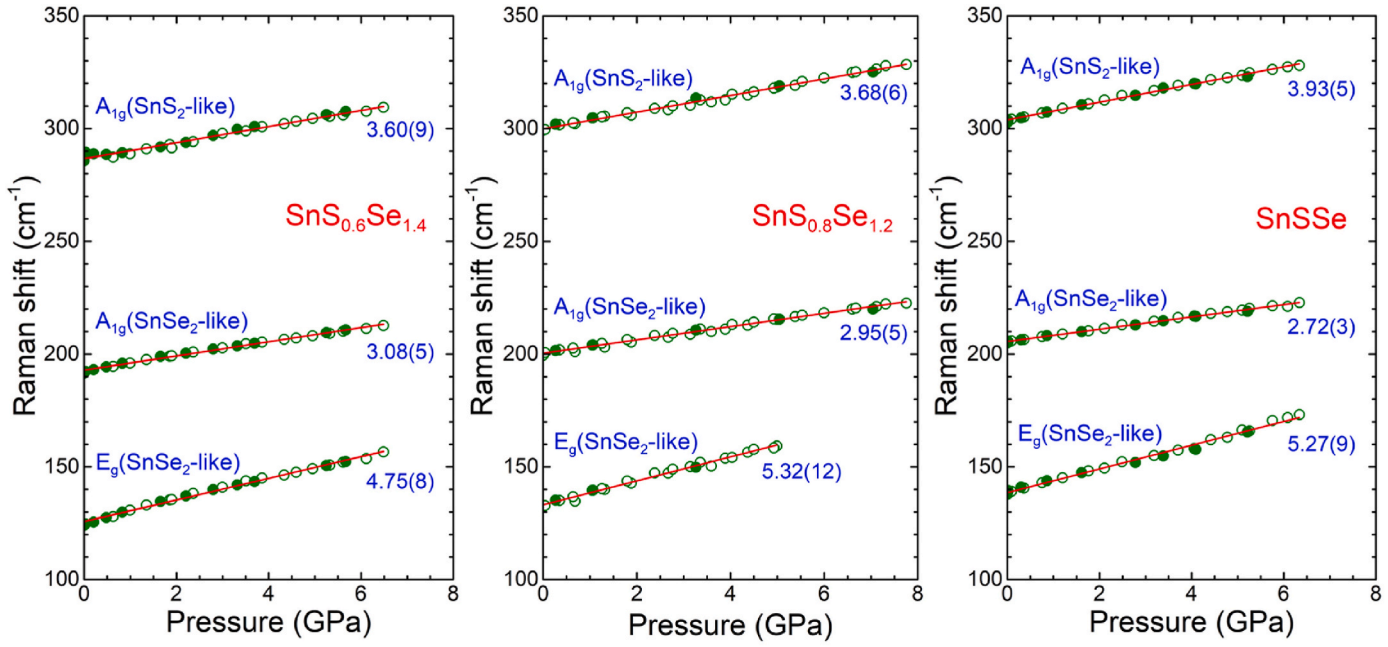

Fig. 4. The frequencies of the main Raman peaks of the ternary SnS_xSe_{2-x} ($x = 0.6, 0.8, 1$) alloys as a function of pressure. Open (solid) symbols correspond to data obtained upon pressure increase (decrease). Lines through the experimental data are their linear least square fits, while numbers refer to the corresponding pressure slopes.

The mode Grüneisen parameters, $\gamma_i = (B/\omega_i)(\partial\omega/\partial P)_i$, where B is the bulk modulus of the material and the index i specifies the mode frequency at ambient conditions and its derivative, represent the thermodynamic and thermoelastic behavior of the condensed matter at high pressure and/or temperature, indicating the influence of anharmonic effects on the phonon spectrum due to the change of the unit cell volume. It has been found experimentally that the bulk moduli for the binary SnS_2 and $SnSe_2$ dichalcogenides are very similar, being 28.1 and 27.3 GPa, respectively [35,36]. Assuming solid solutions formed in the SnS_xSe_{2-x} system, we can linearly interpolate the corresponding bulk modulus to be 27.54, 27.62 and 27.70 GPa for $x = 0.6$, 0.8 and 1, respectively. From the obtained pressure coefficients of the various peak frequencies given in Fig. 4, we extract the Grüneisen parameters for the $A_{1g}(SnS_2$-like) mode: 0.35, 0.34 and 0.36, as well as for the A_{1g} ($SnSe_2$-like) mode: 0.44, 0.41 and 0.37 for $x = 0.6$, 0.8 and 1, respectively. These values indicate the stronger Sn–S interaction along the c-axis compared to that of Sn–Se in the ternary alloys.

4. Conclusion

Summarizing, we have presented herein a detailed study of the hydrostatic pressure response of the E_g($SnSe_2$-like), A_{1g}($SnSe_2$-like) and A_{1g}(SnS_2-like) Raman modes of ternary SnS_xSe_{2-x} ($x = 0.6, 0.8, 1$) tin dichalcogenide crystals. The frequency evolution with pressure of the Raman modes is quasi-linear within the studied pressure range (up to 8 GPa) and fully reversible, confirming the structural stability of tin dichalcogenide alloys. For all the studied compounds, the in-plane E_g($SnSe_2$-like) mode frequency exhibits larger pressure coefficient than those of the A_{1g} modes along the *c*-axis. Moreover, with increasing S content, the pressure coefficient of the A_{1g}(SnS_2-like) mode frequency increases, while that of the A_{1g}($SnSe_2$-like) mode decreases and their Grüneisen parameters suggest a stronger Sn–S interaction along the *c*-axis compared to that of Sn–Se. We expect that the results of the present study will be very informative for future studies regarding the pressure response of the Raman modes of tin dichalcogenide alloys in the nanoscale as a function of the number of layers.

CRediT authorship contribution statement

N. Sorogas: Methodology, Data acquisition & analysis, Writing - original draft. **M. Menelaou**: Experimental support, Data analysis. **A.N. Anagnostopoulos**: Synthesis, Sample characterization. **K. Papagelis**: Experimental support, Writing - review & editing. **D. Christofilos**: Experimental support, Writing - review & editing. **J. Arvanitidis**: Conceptualization, Supervision, Writing - original draft.

Declaration of competing interest

The authors declare that they have no known competing financial interests or personal relationships that could have appeared to influence the work reported in this paper.

Data availability

Data will be made available on request.

Acknowledgements

This research is a part of the doctoral thesis of NS, the implementation of which was co-financed by Greece and the European Union (European Social Fund-ESF) through the Operational Programme "Human Resources Development, Education and Lifelong Learning" in the context of the Act "Enhancing Human Resources Research Potential by undertaking a Doctoral Research" Sub-action 2: IKY Scholarship Programme for PhD candidates in the Greek Universities. The authors also acknowledge the Center of Interdisciplinary Research and Innovation of the Aristotle University of Thessaloniki (CIRI-AUTH) for the access to the Raman instrumentation.

References

[1] P. Shinde, C.S. Rout, Advances in synthesis, properties and emerging applications of tin sulfides and its heterostructures, Mater. Chem. Front. 5 (2021) 516–556.
[2] S. Gedi, V.R.M. Reddy, T.R.R. Kotte, C. Park, W.K. Kim, Fundamental aspects and comprehensive review on physical properties of chemically grown tin-based binary sulfides, Nanomaterials 11 (2021) 1955.
[3] M. Kumar, S. Rani, Y. Singh, K.S. Gour, V.N. Singh, Tin-selenide as a futuristic material: properties and applications, RSC Adv. 11 (2021) 6477–6503.
[4] J. Yao, G. Yang, Van der Waals heterostructures based on 2D layered materials: fabrication, characterization, and application in photodetection, J. Appl. Phys. 131 (2022), 161101.
[5] Y. Bai, X. Zong, H. Yu, Z.G. Chen, L. Wang, Scalable low-cost SnS_2 nanosheets as counter electrode building blocks for dye-sensitized solar cells, Chem. Eur J. 20 (2014) 8670–8676.
[6] C.K. Zankat, P.M. Pataniya, A. Patel, S.A. Bhakhar, S. Narayan, G.K. Solanki, K. D. Patel, V.M. Pathak, C.K. Sumesh, P.K. Jha, Self-powered photodetector based on $SnSe_2$/$MoSe_2$ heterostructure, Mater, Today Energy 18 (2020), 100550.
[7] S. Wei, C. Ge, L. Zhou, S. Zhang, M. Dai, F. Gao, Y. Sun, Y. Qiu, Z. Wang, J. Zhang, P.A. Hu, Performance improvement of multilayered SnS_2 field effect transistors through synergistic effect of vacancy repairing and electron doping introduced by EDTA, ACS Appl. Electron. Mater. 1 (2019) 2380–2388.
[8] A. Qazi, M. Nazir, M. Shahid, S. Butt, M.A. Basit, Facile development of hybrid bulk-nanostructured SnSe/SnS for antibacterial activity with negligible cytotoxicity, J. Cluster Sci. 32 (2020) 665–672.
[9] M. Tannarana, G.K. Solanki, S.A. Bhakhar, K.D. Patel, V.M. Pathak, P.M. Pataniya, 2D-$SnSe_2$ nanosheet functionalized piezo-resistive flexible sensor for pressure and human breath monitoring, ACS Sustain. Chem. Eng. 8 (2020) 7741–7749.
[10] H. Bergeron, D. Lebedev, M.C. Hersam, Polymorphism in post-dichalcogenide two-dimensional materials, Chem. Rev. 121 (2021) 2713–2775.
[11] Y. Wang, Y. Zhao, X. Ding, L. Qiao, Recent advances in the electrochemistry of layered post-transition metal chalcogenide nanomaterials for hydrogen evolution reaction, J. Energy Chem. 60 (2021) 451–479.
[12] B. Pałosz, E. Salje, Lattice parameters and spontaneous strain in AX_2 polytypes: CdI_2, PbI_2, SnS_2 and $SnSe_2$, J. Appl. Crystallogr. 22 (1989) 622–623.
[13] P. Manou, J.A. Kalomiros, A.N. Anagnostopoulos, K. Kambas, Optical Properties of $SnSe_2$ single crystals, MRS Bull. 31 (1996) 1407–1415.
[14] E.P. Trifonova, I.Y. Yanehev, V.B. Stoyanova, S. Mandalidis, K. Kambas, A. N. Anagnostopoulos, Crystal growth and characterization of SnS_2, MRS Bull. 31 (1996) 919–924.
[15] C.R. Whitehouse, A.A. Balchin, Polytypism in tin disulphide, J. Cryst. Growth 47 (1979) 203–212.
[16] J.C. Mikkelsen Jr., Polytype characterization of SnS_2 crystals grown from Sn-rich melts, J. Cryst. Growth 49 (1980) 253–260.
[17] B. Pałosz, W. Palosz, S. Gierlotka, Polytypism of crystals of tin disulphide; Structures of 21 polytypes of SnS_2, Acta Crystallogr. C 41 (1985) 807–811.
[18] R.S. Mitchell, Y. Fujiki, Y. Ishizawa, Structural polytypism of tin disulfide: its relationship to environments of formation, J. Cryst. Growth 57 (1982) 273–279.
[19] T. Minagawa, Common polytypes of SnS_2 and $SnSe_2$, J. Phys. Soc. Jpn. 49 (1980) 2317–2318.
[20] B. Pałosz, Reasons for polytypism of crystals of the type MX_2 II. Clasification of faults and structural series of polytypes; Conditions of polytypic growth of CdI_2, PbI_2, $CdBr_2$, SnS_2, $SnSe_2$ and $Ti_{1.2}S_2$, Phys. Status Solidi A 80 (1983) 11–41.
[21] J.M. Gonzalez, I.I. Oleynik, Layer-dependent properties of SnS_2 and $SnSe_2$ two-dimensional materials, Phys. Rev. B 94 (2016), 125443.
[22] J. Yu, C.Y. Xu, Y. Li, F. Zhou, X.S. Chen, P.A. Hu, L. Zhen, Ternary SnS_{2-x} Se_x alloys nanosheets and nanosheet assemblies with tunable chemical compositions and band gaps for photodetector applications, Sci. Rep. 5 (2015), 17109.
[23] L. Du, C. Wang, W. Xiong, B. Wei, F. Yang, S. Chen, L. Ma, X. Wang, C. Xia, X. Zhang, Z. Wang, Q. Liu, Strain-induced band-gap tuning of 2D-SnSSe flakes for application in flexible Sensors, Adv. Mater. Technol. 5 (2020), 1900853.
[24] S. Dong, Z. Wang, Improving the catalytic activity for hydrogen evolution of monolayered $SnSe_{2(1-x)}S_{2x}$ by mechanical strain, Beilstein J. Nanotechnol. 9 (2018) 1820–1827.
[25] R. Zhang, J. Jiang, W. Wu, Scalably nanomanufactured atomically thin materials-based wearable health sensors, Small Structures 3 (2022), 2100120.
[26] D.Y. Lin, H.P. Hsu, C.F. Tsai, C.W. Wang, Y.T. Shih, Temperature dependent excitonic transition energy and enhanced electron-phonon coupling in layered ternary $SnS_{2-x}Se_x$ semiconductors with fully tunable stoichiometry, Molecules 26 (2021) 2184.
[27] P. Perumal, R.K. Ulaganathan, R. Sankar, Y.M. Liao, T.M. Sun, M.W. Chu, F. C. Chou, Y.T. Chen, M.H. Shih, Y.F. Chen, Ultra-thin layered ternary single crystals $[Sn(S_xSe_{1-x})_2]$ with bandgap engineering for high performance phototransistors on versatile substrates, Adv. Funct. Mater. 26 (2016) 3630–3638.
[28] J. Chen, M. Liu, X. Liu, Y. Ouyang, W. Liu, Z. Wei, The SnSSe SA with high modulation depth for passively Q-switched fiber laser, Nanophotonics 9 (2020) 2549–2555.
[29] G.P. Kafle, C. Heil, H. Paudyal, E.R. Margine, Electronic, vibrational, and electron-phonon coupling properties in $SnSe_2$ and SnS_2 under pressure, J. Mater. Chem. C 8 (2020) 16404–16417.
[30] Y. Zhou, B. Zhang, X. Chen, C. Gu, C. An, Y. Zhou, K. Cai, Y. Yuan, C. Chen, H. Wu, R. Zhang, C. Park, Y. Xiong, X. Zhang, K. Wang, Z. Yang, Pressure-induced metallization and robust superconductivity in pristine 1T-$SnSe_2$, Adv. Electron. Mater. 4 (2018), 1800155.
[31] B. Yue, W. Zhong, X. Yu, F. Hong, Superconductivity in the van der Waals crystal SnS_2 up to 105 GPa, Phys. Rev. B 105 (2022), 104514.
[32] J. Ying, H. Paudyal, C. Heil, X.J. Chen, V.V. Struzhkin, E.R. Margine, Unusual pressure-induced periodic lattice distortion in $SnSe_2$, Phys. Rev. Lett. 121 (2018), 027003.
[33] M.J. Powell, The effect of pressure on the optical properties of 2H and 4H SnS_2, J. Phys. C Solid State Phys. 10 (1977) 2967–2977.
[34] M.J. Powell, W.Y. Liang, D.J. Chadi, Pressure dependence of the band structure of 2H-SnS_2, J. Phys. C Solid State Phys. 11 (1978) 885–894.
[35] M. Filsø, E. Eikeland, J. Zhang, S.R. Madsen, B.B. Iversen, Atomic and electronic structure transformations in SnS_2 at high pressures: a joint single crystal X-ray diffraction and DFT study, Dalton Trans. 45 (2016) 3798–3805.
[36] Z.V. Borges, C.M. Poffo, J.C. de Lima, S.M. Souza, D.M. Trichês, R.S. de Biasi, High-pressure angle-dispersive X-ray diffraction study of mechanically alloyed $SnSe_2$, J. Appl. Phys. 124 (2018), 215901.
[37] S.V. Bhatt, M.P. Deshpande, V. Sathe, S.H. Chaki, Effect of pressure and temperature on Raman scattering and an anharmonicity study of tin dichalcogenide single crystals, Solid State Commun. 201 (2015) 54–58.
[38] A.N. Utyuzh, Y.A. Timofeev, G.N. Stepanov, Effect of pressure on Raman spectra of SnS_2 single crystals, Phys. Solid State 52 (2010) 352–356.

[39] K. Nguyen-Cong, J.M. Gonzalez, B.A. Steele, I.I. Oleynik, Tin-selenium compounds at ambient and high pressures, J. Phys. Chem. C 122 (2018) 18274–18281.
[40] X. Zhang, L. Dai, H. Hu, M. Hong, C. Li, Pressure-induced coupled structural-electronic transition in SnS_2 under different hydrostatic environments up to 39.7 GPa, RSC Adv. 12 (2022) 2454–2461.
[41] Y. Shi, H. Song, N. Li, X. Wu, K. Wang, Y. Wu, G. Ye, H. Huang, High-pressure structural stability and bandgap engineering of layered tin disulfide, Appl. Phys. Lett. 121 (2022), 114101.
[42] M. de Oliveira Melquiades, L.S. de Oliveira, R.A. da Silva, S.M. de Souza, M. O. Orlandi, Structural, thermal, vibrational, and optical characterization of Sn-S-Se dichalcogenide system synthesized by high-energy ball milling, J. Phys. Chem. Solids 157 (2021), 110203.
[43] H. Zhao, Y. Yan, C. Xia, X. Song, A. Dong, J. Su, J. Li, Layered $SnSe_xS_{2-x}$ alloys with fully chemical compositions and band gaps for photoelectrochemical water oxidation, J. Phys. D Appl. Phys. 53 (2020), 185101.
[44] A.K. Garg Chanchal, MREI-model calculations of optical phonons in layered mixed crystals of 2H-polytype of the series $SnS_{2-x}Se_x$ ($0 \leq x \leq 2$), Physica B 383 (2006) 188–193.
[45] V.G. Hadjiev, D. De, H.B. Peng, J. Manongdo, A.M. Guloy, Phonon probe of local strains in SnS_xSe_{2-x} mixed crystals, Phys. Rev. B 87 (2013), 104302.
[46] A.K. Garg, Concentration dependent vibrational mode behaviour in the mixed crystal system SnS_xSe_{2-x}, J. Mol. Struct. 247 (1991) 47–60.
[47] M.M. Gospodinov, V. Marinova, E. Polychroniadis, D. Papadopoulos, K. Kampas, A. N. Anagnostopoulos, K. Kyritsi, Growth and characterization of $(SnS_2)_x$-$(SnSe_2)_{1-x}$ mixed crystals, MRS Bull. 38 (2003) 177–184.
[48] A. Mujica, A. Rubio, A. Muñoz, R.J. Needs, High-pressure phases of group-IV, III-V, and II-VI compounds, Rev. Mod. Phys. 75 (2003) 863–912.
[49] A. Jayaraman, Diamond anvil cell and high-pressure physical investigations, Rev. Mod. Phys. 55 (1983) 65–108.
[50] A.J. Smith, P.E. Meek, W.Y. Liang, Raman scattering studies of SnS_2 and $SnSe_2$, J. Phys. C Solid State Phys. 10 (1977) 1321–1333.
[51] S. Nakashima, H. Katahama, A. Mitsuishi, The effect of polytypism on the vibrational properties of SnS_2, Phys. B+C 1–3 (1981) 343–346.
[52] Y. Huang, E. Sutter, J.T. Sadowski, M. Cotlet, O.L.A. Monti, D.A. Racke, M. R. Neupane, D. Wickramaratne, R.K. Lake, B.A. Parkinson, P. Sutter, Tin disulfide-an emerging layered metal dichalcogenide semiconductor: materials properties and device characteristics, ACS Nano 8 (2014) 10743–10755.
[53] Y. Wang, L. Huang, B. Li, J. Shang, C. Xia, C. Fan, H.X. Deng, Z. Wei, J. Li, Composition-tunable 2D $SnSe_{2(1-x)}S_{2x}$ alloys towards efficient bandgap engineering and high performance (opto)electronics, J. Mater. Chem. C 5 (2016) 84–90.